Editors' Suggestion

Pattern Propagation Driven by Surface Curvature

Ryosuke Nishide[1,*] and Shuji Ishihara[1,2,†]
[1]Graduate School of Arts and Sciences, The University of Tokyo, Komaba 3-8-1, Meguro-ku, Tokyo 153-8902, Japan
[2]Universal Biology Institute, The University of Tokyo, Komaba 3-8-1, Meguro-ku, Tokyo 153-8902, Japan

(Received 9 February 2022; accepted 15 April 2022; published 2 June 2022)

Pattern dynamics on curved surfaces are found everywhere in nature. The geometry of surfaces has been shown to influence dynamics and play a functional role, yet a comprehensive understanding is still elusive. Here, we report for the first time that a static Turing pattern on a flat surface can propagate on a curved surface, as opposed to previous studies, where the pattern is presupposed to be static irrespective of the surface geometry. To understand such significant changes on curved surfaces, we investigate reaction-diffusion systems on axisymmetric curved surfaces. Numerical and theoretical analyses reveal that both the symmetries of the surface and pattern participate in the initiation of pattern propagation. This study provides a novel and generic mechanism of pattern propagation that is caused by surface curvature, as well as insights into the general role of surface geometry.

DOI: 10.1103/PhysRevLett.128.224101

Pattern formation and dynamics on curved surfaces are ubiquitous, particularly in biological systems [1–3]. Recent studies reveal the functional roles of the topology and geometry of surfaces in pattern formation [4–7]. For example, defect dynamics on closed curved surfaces are constrained by the Poincaré-Hopf theorem and have been investigated in liquid crystals [8], flocking [9], and active nematics [10]. Such defects in cortical actin fibers serve as organization centers in the morphogenesis of hydra regeneration [4]. Molecules such as Bin/Amphiphysin/Rvs domain proteins sense the curvature of a cellular membrane and regulate the cellular shape [11]. Cellular migration is guided by the curvature of a substrate, which is a response known as "curvotaxis" [5]. It was theoretically shown that surface curvature can induce splitting [6] and rectification [12] of excitable waves. Rectification by curved surfaces has been reported in the collective motion of self-propelled particles [13]. However, a comprehensive and general understanding of the effect of surface geometry on pattern dynamics and its functional role remains elusive.

Among pattern formation, Turing patterns are a prominent example arising from reaction-diffusion systems [14–17]. Turing patterns on curved surfaces [18–20], such as spheres [14,21–25], hemispheres [26,27], toruses [25,28], ellipsoids [28,29], and deformed (but axisymmetric) cylinders and spheres [30] have been investigated previously. These studies revealed how the Turing instability condition changes from the flat plane case and how the position of the pattern is modulated by the inhomogeneity of the surface curvature [19], which is referred to as "pinning" by Frank *et al.* [30]. It is noteworthy that in these studies, the Turing pattern, which is static on a flat plane, was assumed to remain static irrespective of the surface geometry. However, this assumption has not been validated so far [31].

We conducted numerical simulations using the Brusselator [32] and Lengyel-Epstein (LE) models [33,34] on several curved surfaces with a parameter set indicating Turing instability for flat planes (see Supplemental Material [35] for simulation details). We observed that the static pattern on a flat surface becomes a propagating pattern on several curved surfaces (see Fig. 1, and Videos 1 and 2 in the Supplemental Material [35]), indicating that a surface

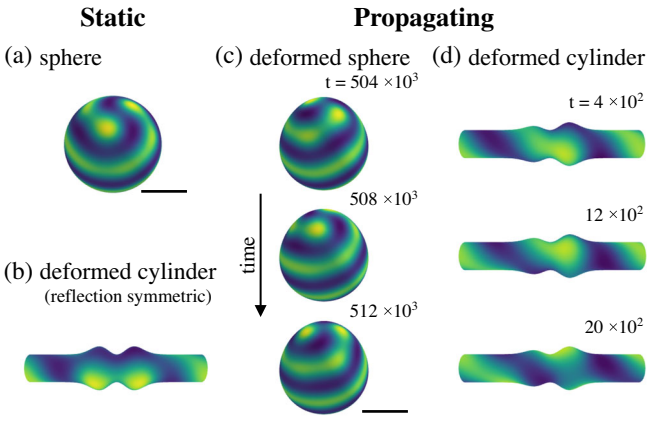

FIG. 1. Propagating and static patterns on surfaces. Concentration u obtained from numerical simulations of the Brusselator model are indicated by color scale. Lighter (darker) colors represent higher (lower) concentrations. Parameters are set as $(a, b, D_u, D_v) = (2.0, 4.5, 0.5, 1.8)$. (a),(b) Static patterns on sphere (a) and reflection-symmetric deformed cylinder (b). (c), (d) Propagating patterns appear on deformed spheres (c) and deformed cylinders (d). See Videos 1 and 2 [35] for spherical and cylindrical cases, respectively. Periodic boundary conditions are used for cylindrical surfaces. Scale bars: six simulation length units. For deformed cylinders, axial length is 4π. See Supplemental Material [35] for detailed descriptions of these surfaces.

curvature can result in the dynamic motion of patterns, unlike what has been thought thus far. The simulation results suggest that the surface symmetry contributes to the propagation; for example, the pattern remains static on a reflection-symmetric cylindrical surface [see Fig. 1(b)], whereas a moving pattern appears on a cylindrical surface without reflection symmetry [see Fig. 1(d)]. In addition, propagating waves are observed in both the Brusselator and LE models, which suggests a generic mechanism underlies this phenomenon.

To systematically investigate the propagation dynamics based on the surface curvature, we analyzed a reaction-diffusion system on an axisymmetric surface parametrized as $\boldsymbol{r} = [x, r(x)\cos\theta, r(x)\sin\theta]$. x and θ are defined as $-2\pi \le x < 2\pi$ and $0 \le \theta < 2\pi$, respectively, for which periodic boundary conditions are employed. Unless otherwise mentioned, we set $r(x) = d + k_1\cos(x) + k_2\cos(2x - \gamma\pi/2)$ with $d = 1.7$, $k_1 = 0.3$, and $k_2 = 0.05$ [see Fig. 2(a)]. γ controls the reflection symmetry of the surface about $x = 0$; i.e., $r(x) = r(-x)$ holds at $\gamma = 0$ but not for $\gamma \neq 0$ [see Fig. 2(b)]. Herein, we focus on the numerical results obtained using the Brusselator model,

$$\begin{aligned} \partial_t u &= D_u \Delta u + u^2 v - bu - u + a, \\ \partial_t v &= D_v \Delta v - u^2 v + bu, \end{aligned} \tag{1}$$

where u and v represent chemical concentrations and are functions of the position on the surface (x, θ) and time t. On a curved surface, the diffusion terms in Eq. (1) are described by the Laplace-Beltrami operator Δ [18,37]. For the axisymmetric surface, Δ is expressed as

$$\Delta \bullet = \frac{1}{r\sqrt{1 + r'^2}} \partial_x \left(\frac{r}{\sqrt{1 + r'^2}} \partial_x \bullet \right) + \frac{1}{r^2} \partial_\theta^2 \bullet, \tag{2}$$

where r' represents $dr(x)/dx$. The surface on a normal cylinder is equivalent to a flat plane, since they have the same metric. By choosing the appropriate parameter set, the system becomes Turing unstable, as indicated by the dispersion relation $\mu(\lambda)$ and numerical simulations on a flat plane [see Figs. 2(c) and 2(d)]. The dispersion relation $\mu(\lambda)$ is obtained via linear stability analysis in the uniform state $(u, v) = (a, b/a)$ and represents the growth rate of a mode characterized by λ, where λ is an eigenvalue of the Laplace-Beltrami operator determined by $\Delta\phi = -\lambda\phi$ (see Supplemental Material [35]). For flat surfaces, λ coincides with the square of the wave number. $\mu(\lambda)$ in Fig. 2(c) takes real positive values between a finite range of λ exhibiting a typical form of Turing instability. Note that the dispersion relation $\mu(\lambda)$, and thus the Turing condition, is the same for any surface [18].

We performed numerical simulations by varying γ. When the pattern is helical stripes on a reflection-symmetric surface, the dynamics become static, as shown in Fig. 3(a) ($\gamma = 0$) and Video 3 [35]. As the reflection

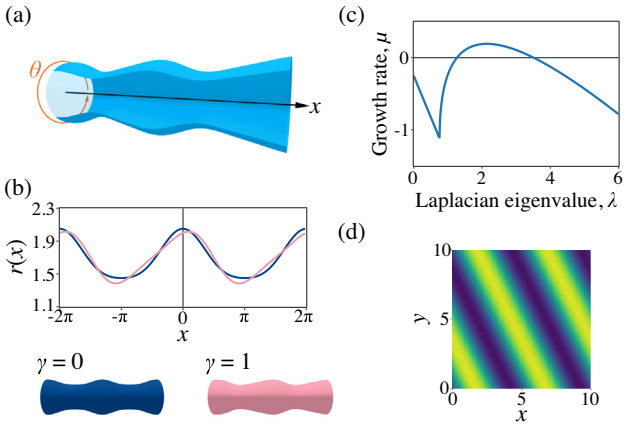

FIG. 2. Propagation of stripe patterns on axisymmetric surfaces. (a), (b) Axisymmetric surface whose radius is $r(x) = d + k_1\cos(x) + k_2\cos(2x - \gamma\pi/2)$. γ represents the parameter for controlling surface reflection asymmetry along the x axis. Surfaces at $\gamma = 0$ and 1 are shown by dark blue and light red lines in panel (b), respectively. (c) Dispersion relation with parameter set $(a, b, D_u, D_v) = (2.0, 4.5, 0.5, 1.8)$. (d) Turing pattern on flat plane with parameter set shown in (c).

symmetry of the surface is diminished owing to changes in γ, pattern propagation emerges, as shown in Fig. 3(a) ($\gamma = 1$) and Video 3 [35]. The velocity of the propagation is plotted against γ in Fig. 3(b) (blue points). The propagation velocity is proportionally dependent on γ in the vicinity of $\gamma = 0$, indicating that slight reflection asymmetry is sufficient to trigger propagation. Depending on the parameter and initial conditions, stripes almost parallel along the x axis can appear [see Fig. 3(c)]. For such a pattern, we do not observe propagation for any value of γ.

Dotted patterns also appeared via Turing instability [see Fig. S1(b) in the Supplemental Material [35]]. On the axisymmetric surface, we observed dotted patterns that are aligned helically [Fig. 3(d)] and parallelly along the x axis [Fig. 3(f)]. The helically aligned dots pattern remains static on the reflection-symmetric surface at $\gamma = 0$ but propagates at $\gamma \neq 0$ [see Figs. 3(d) and 3(e), and Video 4 in the Supplemental Material [35]]. By contrast, the parallelly aligned dots patterns remain static for any value of γ [see Fig. 3(f)]. Similar results for the stripe and dotted patterns are obtained in simulations based on other parameter sets and in the LE model (see Fig. S2 in the Supplemental Material [35]), as well as on surfaces with different forms of $r(x)$ [see Figs. 1(b) and 1(d)]. These observations suggest that the reflection asymmetry of the surface and profile of the pattern are both responsible for the initiation of pattern propagation.

To analyze these numerical results, we examined the observed patterns in terms of symmetry; see the projected concentration profile of $u(x, \theta)$ at a late-time point t on the x-θ plane in Figs. 4(a)–4(d). The patterns obtained in the simulations can be classified into two types (Fig. S3 [35]). One is referred to as reflection-symmetric patterns about

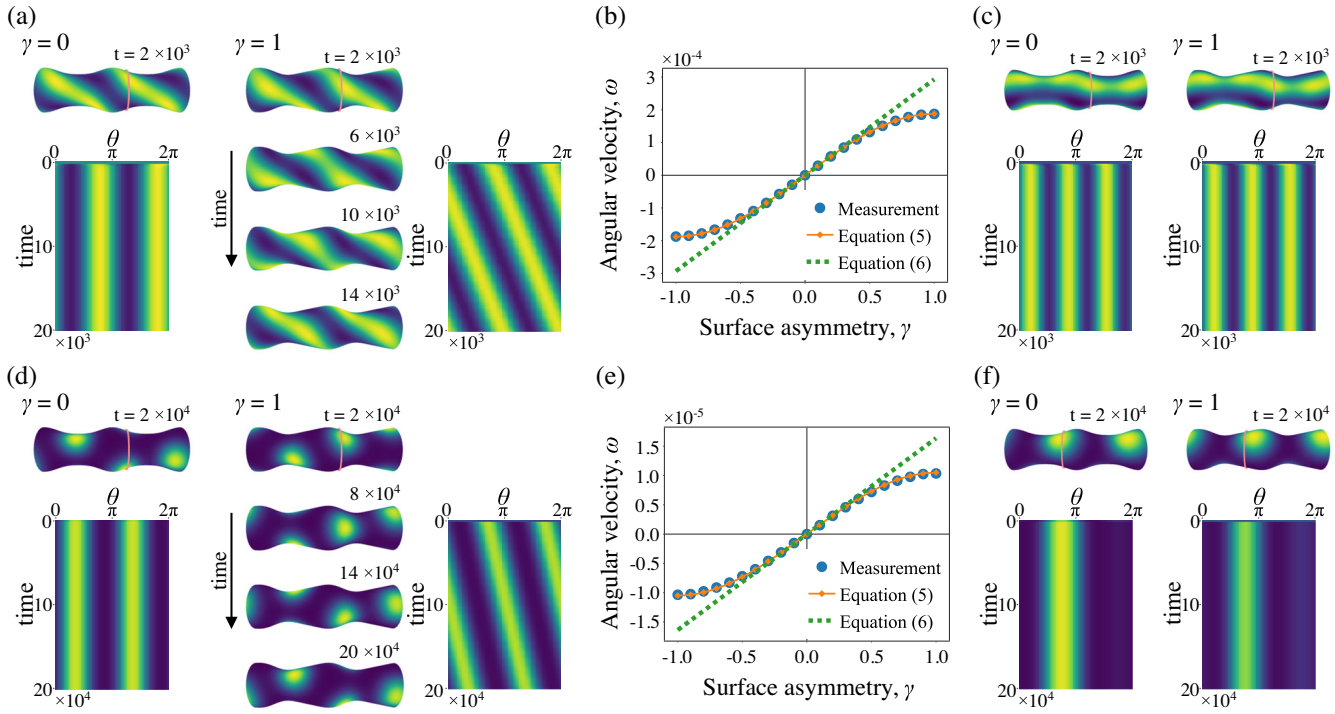

FIG. 3. Propagation of stripe and dotted patterns on axisymmetric surfaces. (a) Helical stripe patterns on reflection-symmetric ($\gamma = 0$) and asymmetric ($\gamma = 1$) surfaces (Video 3 [35]). Kymographs of these patterns along the θ axis (indicated by pale red line) are shown. (b) Angular velocity ω of propagating pattern along the θ axis against surface asymmetry γ. ω is obtained via three different methods: direct measurement (blue point), velocity relation equation (5) (orange line), and perturbative velocity relation equation (6) (dashed green line). (c) Parallel stripe patterns along the x axis on reflection-symmetric (left) and asymmetric (right) surfaces. (d)–(f) Date equivalent to (a)–(c) for helically aligned dots patterns [(d),(e); Video 4 [35]] and for parallelly aligned dots patterns (f). Parameter sets of patterns are $(a, b, D_u, D_v) = (2.0, 4.5, 0.5, 1.8)$ (a), (2.8, 5.0, 0.4, 2.4) (c), (1.5, 2.5, 0.3, 3.0) (d), and (1.5, 3.0, 0.5, 3.5) (f) (see also Fig. S1 in the Supplemental Material [35]).

the θ axis, where the patterns are exactly invariant by reflection about the θ axis with an appropriate reflection axis and translation along the x axis by an integer multiple of 2π satisfying $u(x, \theta) = u(x + 2n\pi, -\theta + \theta_0)$ with appropriate values of θ_0 and integer n [see Figs. 4(a) and 4(c)]. Such patterns include the "parallel stripes" and "parallelly aligned dots" along the x axis mentioned above [see Figs. 3(c) and 3(f)], and they remain static. The other patterns include the "helical stripes" and "helically aligned dots" [see Figs. 3(a) and 3(d)] that appear to be inversion symmetric about the θ and x axes [see Figs. 4(b) and 4(d)]. However, the inversion symmetry holds exactly only at $\gamma = 0$, where the patterns satisfy $u(x, \theta) = u(-x + 2n\pi, -\theta + \theta_0)$ with appropriate θ_0 and n values. For $\gamma \neq 0$, the inversion symmetry is merely an approximation. Thus, the absence of the inversion-symmetric solution is the key to the emergence of propagation.

Based on the feature of symmetry described above, we performed a theoretical analysis to clarify the mechanism of pattern propagation on curved surfaces. A reaction-diffusion system is generally expressed as

$$\partial_t \boldsymbol{U} = D\Delta \boldsymbol{U} + \boldsymbol{R}(\boldsymbol{U}), \tag{3}$$

where $\boldsymbol{U}$ is a vector composed of the chemical concentration, D is a diagonal diffusion matrix, and $\boldsymbol{R}(\boldsymbol{U})$ is a vector of reaction terms. Using variable $\rho \equiv \theta - \omega t$, the propagating solution along the θ axis is expressed as $\boldsymbol{U}(x, \theta, t) = \boldsymbol{U}(x, \rho)$. Subsequently, Eq. (3) for the propagating solution reads

$$\omega \partial_\rho \boldsymbol{U} + D\Delta \boldsymbol{U} + \boldsymbol{R}(\boldsymbol{U}) = 0. \tag{4}$$

By taking the inner product with $\partial_\rho \boldsymbol{U}$ and integrating over the surface, we obtain

$$\omega = -\frac{\int dS \partial_\rho \boldsymbol{U}^T \boldsymbol{R}}{\int dS (\partial_\rho \boldsymbol{U})^2}, \tag{5}$$

where $dS \equiv r\sqrt{1 + r'^2} dx d\rho$ is a surface area element (see Supplemental Material [35]). This relationship is consistent with the simulation data, as shown by the orange lines in Figs. 3(b) and 3(e). Note that for relaxation systems where the reaction terms are expressed by the gradient of an energy function $H(\boldsymbol{U})$ as $\boldsymbol{R}(\boldsymbol{U}) = -\partial H(\boldsymbol{U})/\partial \boldsymbol{U}$, one can easily prove that $\omega = 0$ using Eq. (5); this indicates that

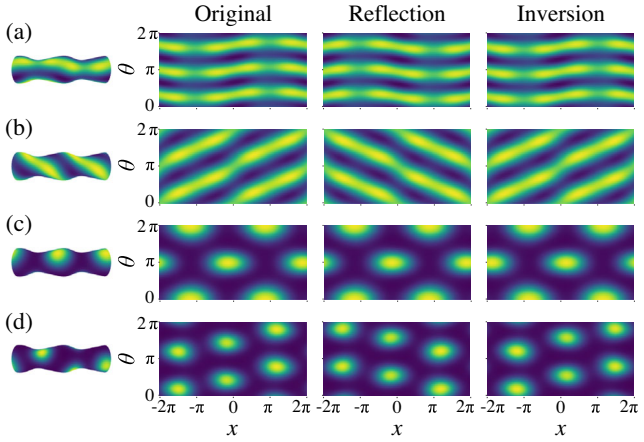

FIG. 4. Relationship between pattern symmetry and pattern propagation. (a)–(d) (First and second columns) patterns on surface and projected images on the x-θ planes, respectively. γ is set to 1.0. (Third column) patterns obtained by reflecting original patterns along the θ axis. (Fourth column) patterns obtained by inverting the original patterns. For ease of comparison, the images in the third and fourth columns are translated along the x and θ axes such that the surface is invariant (i.e., $x \to x + 2n\pi$ and $\theta \to \theta + \theta_0$). (a) Parallel stripes along the x axis; (b) helical stripes; (c) parallelly aligned dots along the x axis; (d) helically aligned dots.

propagation is realizable only in out-of-equilibrium systems.

Equation (5) relates propagation velocity to the pattern profile and surface geometry. Considering a pattern with reflection symmetry about the θ axis [a pattern satisfying $\boldsymbol{U}(x,\rho) = \boldsymbol{U}(x + 2n\pi, -\rho + \rho_0)$ with appropriate n and ρ_0], $\boldsymbol{R}(\boldsymbol{U})$ satisfies the same symmetry. Subsequently, owing to the parity of $\partial_\rho \boldsymbol{U}$ and $\boldsymbol{R}(\boldsymbol{U})$, the integral in the numerator of the equation vanishes, and accordingly, $\omega = 0$ for such a pattern. This applies similarly to the case for a helical inversion-symmetric pattern at $\gamma = 0$, which satisfies $\boldsymbol{U}(x,\rho) = \boldsymbol{U}(-x + 2n\pi, -\rho + \rho_0)$. These arguments prove the absence of propagation in parallel stripes and parallelly aligned dots patterns along the x axis for any value of γ, as well as in helical patterns at $\gamma = 0$. By contrast, for a helical pattern with $\gamma \neq 0$, these symmetries do not hold, and in general, ω is finite, as shown below.

To investigate the mechanism by which propagation occurs due to the breaking of reflection symmetry of the surface geometry, we performed a perturbation analysis by setting the radius of the axisymmetric surface to $r(x) = r_0(x) + \epsilon r_1(x)$ (see Supplemental Material [35] for details regarding the perturbation analysis). An even function $r_0(x)$ represents the reflection-symmetric part of the surface, whereas an odd function $r_1(x)$ represents the asymmetric part. For a small ϵ, the Laplace-Beltrami operator is expanded to $\Delta = \Delta_0 + \epsilon\bar{\Delta}_1 + \mathcal{O}(\epsilon^2)$, where Δ_0 is the operator for reflection-symmetric surfaces, and $\epsilon\bar{\Delta}_1$ represents modulation via asymmetric deformation. Δ_0 and $\bar{\Delta}_1$ exhibit the opposite parity for reflection about the x axis; i.e., they change as $\Delta_0 \to \Delta_0$ and $\bar{\Delta}_1 \to -\bar{\Delta}_1$, respectively, for a transformation $x \to -x$. At $\epsilon = 0$, we assume that the system shows a helical pattern $\boldsymbol{U}_0$ satisfying inversion symmetry $\boldsymbol{U}_0(x,\rho) = \boldsymbol{U}_0(-x + 2n\pi, -\rho + \rho_0)$, for which the velocity vanishes as discussed above. The effect of asymmetric surface deformation on the pattern propagation dynamics is evaluated as follows:

$$\omega = -\epsilon \frac{\int dS_0 \boldsymbol{W}_0^T D\bar{\Delta}_1 \boldsymbol{U}_0}{\int dS_0 \boldsymbol{W}_0^T \partial_\rho \boldsymbol{U}_0} + \mathcal{O}(\epsilon^2), \tag{6}$$

where $dS_0 \equiv r_0\sqrt{1 + r_0'^2}dxd\rho$ and function vector $\boldsymbol{W}_0$ are determined by the system at $\epsilon = 0$. Owing to the parity of $\bar{\Delta}_1$, Eq. (6) does not vanish in general, indicating that the loss of reflection symmetry of the surface about the x axis causes the propagation of the Turing pattern. We numerically verified the relationship above based on our simulation data by setting $r_0(x) = d + k_1\cos(x) + k_2\cos(2x)$, $r_1(x) = (\pi k_2/2)\sin(2x)$, and $\epsilon = \gamma$, and discovered good agreement in the vicinity of $\epsilon = 0$ [Figs. 3(b) and 3(e), dashed green lines]. Taken together, these analyses corroborate the emergence of Turing patterns propagating on curved surfaces.

It is noteworthy that the analyses above do not exclude a moving Turing pattern on a highly symmetric surface if the pattern is out of symmetry. In our numerical simulations, we observed a stripe pattern propagating on a spherical surface in some cases, where the pattern does not satisfy the symmetry expected from the surface (see Fig. S4 in the Supplemental Material [35]).

In summary, we discovered chemical waves that propagated genuinely driven by surface curvature. This propagation does not occur in one-dimensional systems, where no intrinsic curvature exists, which contrasts with typical propagating waves such as those in excitable media, where the initiation of wave propagation is independent of the surface geometry. By performing numerical simulations and perturbative analysis, we identified the generic conditions for pattern propagation irrespective of the model equations for axisymmetric surfaces, where loss of surface reflection symmetry along the x axis results in a loss of pattern inversion symmetry and propagation along the θ axis. The (a)symmetry of the surface and pattern are both important, suggesting that in general surfaces, pattern dynamics is determined by the geometric feature of the surface and pattern profile. The pattern propagation discovered in this Letter was overlooked previously, likely because most of those previous studies focused primarily on highly symmetric surfaces. In addition, the propagation velocity is generally much slower than that of pattern formation at the early stage; for example, in Fig. S4 of the Supplemental Material [35], images are shown every 1.0×10^4 simulation time units (STU), whereas the development of the pattern is shorter than 1.0×10^3 STU

[see also very early stages $t < 10^3$ of the simulations shown in kymographs of Figs. 3(a) and 3(d)].

Our findings imply the new roles of surface geometry for pattern dynamics applicable to natural and engineering systems. For example, geometry-dependent information transduction is possible in a growing organ, where deformation of the surface can cause initiation (or suppression) of wave propagation, which can subsequently result in the feedback regulation of organ growth. Similar regulation between pattern and surface geometry is possible in the molecular localization on the cell membrane, either inside or outside the surface. In the future, our study should be extended to general curved surfaces and network systems [38], including deformable surfaces [37,39,40]. Furthermore, it would be interesting to investigate similar phenomena in systems other than reaction-diffusion systems, such as active matter systems with polar and nematic orders.

We thank T. Namba, M. Tateno, and N. Saito for their fruitful comments. This study was supported by Japan Society for the Promotion of Science KAKENHI Grant No. JP18H01185, No. JPJSJPR20191501, and Japan Science and Technology Agency Core Research for Evolutional Science and Technology Grant No. JPMJCR1923, Japan (to S. I.) and by Japan Science and Technology Support for Pioneering Research Initiated by the Next Generation Grant No. JPMJSP2108 (to R. N.).

*r-nishide2018@g.ecc.u-tokyo.ac.jp
†csishihara@g.ecc.u-tokyo.ac.jp

[1] T. H. Tan, J. Liu, P. W. Miller, M. Tekant, J. Dunkel, and N. Fakhri, Topological turbulence in the membrane of a living cell, Nat. Phys. **16**, 657 (2020).
[2] J. Bischof, C. A. Brand, K. Somogyi, I. Májer, S. Thome, M. Mori, U. S. Schwarz, and P. Lénárt, A cdk1 gradient guides surface contraction waves in oocytes, Nat. Commun. **8**, 849 (2017).
[3] S. Alonso, M. Bär, and B. Echebarria, Nonlinear physics of electrical wave propagation in the heart: A review, Rep. Prog. Phys. **79**, 096601 (2016).
[4] Y. Maroudas-Sacks, L. Garion, L. Shani-Zerbib, A. Livshits, E. Braun, and K. Keren, Topological defects in the nematic order of actin fibres as organization centres of *hydra* morphogenesis, Nat. Phys. **17**, 251 (2021).
[5] L. Pieuchot *et al.*, Curvotaxis directs cell migration through cell-scale curvature landscapes, Nat. Commun. **9**, 3995 (2018).
[6] K. Horibe, K. Hironaka, K. Matsushita, and K. Fujimoto, Curved surface geometry-induced topological change of an excitable planar wavefront, Chaos **29**, 093120 (2019).
[7] N. Saito and S. Sawai, Three-dimensional morphodynamic simulations of macropinocytic cups, iScience **24**, 103087 (2021).
[8] S. Kralj, R. Rosso, and E. G. Virga, Curvature control of valence on nematic shells, Soft Matter **7**, 670 (2011).
[9] S. Shankar, M. J. Bowick, and M. C. Marchetti, Topological Sound and Flocking on Curved Surfaces, Phys. Rev. X **7**, 031039 (2017).
[10] F. C. Keber, E. Loiseau, T. Sanchez, S. J. Decamp, L. Giomi, M. J. Bowick, M. C. Marchetti, Z. Dogic, and A. R. Bausch, Topology and dynamics of active nematic vesicles, Science **345**, 1135 (2014).
[11] B. Antonny, Mechanisms of membrane curvature sensing, Annu. Rev. Biochem. **80**, 101 (2011).
[12] V. A. Davydov, V. G. Morozov, and N. V. Davydov, Ring-shaped autowaves on curved surfaces, Phys. Lett. A **267**, 326 (2000).
[13] B. Q. Ai, W. J. Zhu, and J. J. Liao, Collective transport of polar active particles on the surface of a corrugated tube, New J. Phys. **21**, 093041 (2019).
[14] A. M. Turing, The chemical basis of morphogenesis, Phil. Trans. R. Soc. B **237**, 37 (1952).
[15] S. Kondo and T. Miura, Reaction-diffusion model as a framework for understanding biological pattern formation, Science **329**, 1616 (2010).
[16] J. Raspopovic, L. Marcon, L. Russo, and J. Sharpe, Digit patterning is controlled by a Bmp-Sox9-Wnt Turing network modulated by morphogen gradients, Science **345**, 566 (2014).
[17] S. Ishihara and K. Kaneko, Turing pattern with proportion preservation, J. Theor. Biol. **238**, 683 (2006).
[18] R. G. Plaza, F. Sánchez-Garduño, P. Padilla, R. A. Barrio, and P. K. Maini, The effect of growth and curvature on pattern formation, J. Dyn. Differ. Equ. **16**, 1093 (2004).
[19] G. Vandin, D. Marenduzzo, A. B. Goryachev, and E. Orlandini, Curvature-driven positioning of Turing patterns in phase-separating curved membranes, Soft Matter **12**, 3888 (2016).
[20] L. Charette, Pattern formation on curved surfaces, Ph.D. thesis, The University of British Columbia, 2019.
[21] C. Varea, J. L. Aragón, and R. A. Barrio, Turing patterns on a sphere, Phys. Rev. E **60**, 4588 (1999).
[22] P. C. Matthews, Pattern formation on a sphere, Phys. Rev. E **67**, 036206 (2003).
[23] M. Núñez-López, G. Chacón-Acosta, and J. A. Santiago, Diffusion-driven instability on a curved surface: Spherical case revisited, Braz. J. Phys. **47**, 231 (2017).
[24] D. Lacitignola, B. Bozzini, M. Frittelli, and I. Sgura, Turing pattern formation on the sphere for a morphochemical reaction-diffusion model for electrodeposition, Commun. Nonlinear Sci. Numer. Simul. **48**, 484 (2017).
[25] F. Sánchez-Garduño, A. L. Krause, J. A. Castillo, and P. Padilla, Turing-Hopf patterns on growing domains: The torus and the sphere, J. Theor. Biol. **481**, 136 (2019).
[26] S. S. Liaw, C. C. Yang, R. T. Liu, and J. T. Hong, Turing model for the patterns of lady beetles, Phys. Rev. E **64**, 041909 (2001).
[27] W. Nagata, H. R. Z. Zangeneh, and D. M. Holloway, Reaction-diffusion patterns in plant tip morphogenesis: Bifurcations on spherical caps, Bull. Math. Biol. **75**, 2346 (2013).
[28] S. Nampoothiri and A. Medhi, Role of curvature and domain shape on Turing patterns, arXiv:1705.02119.
[29] S. Nampoothiri, Effect of geometry on the positioning of a single spot in reaction-diffusion systems, arXiv:1909.06528.

[30] J. R. Frank, J. Guven, M. Kardar, and H. Shackleton, Pinning of diffusional patterns by non-uniform curvature, Europhys. Lett. **127**, 48001 (2019).
[31] A. L. Krause, E. A. Gaffney, P. K. Maini, and V. Klika, Modern perspectives on near-equilibrium analysis of Turing systems, Phil. Trans. R. Soc. A **379**, 20200268 (2021).
[32] G. Nicolis and I. Prigogine, *Self-Organization in Non-equilibrium Systems* (Wiley, New York, 1977).
[33] I. Lengyel and I. R. Epstein, Modeling of Turing structures in the chlorite-iodide-malonic acid-starch reaction system, Science **251**, 650 (1991).
[34] T. Bánsági Jr. and A. F. Taylor, Helical Turing patterns in the Lengyel-Epstein model in thin cylindrical layers, Chaos **25**, 064308 (2015).
[35] See Supplemental Material at http://link.aps.org/supplemental/10.1103/PhysRevLett.128.224101 for details of simulation method, calculation, supplemental figures, and videos which includes Ref. [36].
[36] G. Xu, Discrete Laplace-Beltrami operator on sphere and optimal spherical triangulations, International Journal of Computational Geometry and Applications **16**, 75 (2006).
[37] A. L. Krause, M. A. Ellis, and R. A. Van Gorder, Influence of curvature, growth, and anisotropy on the evolution of Turing patterns on growing manifolds, Bull. Math. Biol. **81**, 759 (2019).
[38] H. Nakao and A. S. Mikhailov, Turing patterns in network-organized activator-inhibitor systems, Nat. Phys. **6**, 544 (2010).
[39] N. Tamemoto and H. Noguchi, Pattern formation in reaction-diffusion system on membrane with mechanochemical feedback, Sci. Rep. **10**, 19582 (2020).
[40] P. W. Miller, N. Stoop, and J. Dunkel, Geometry of Wave Propagation on Active Deformable Surfaces, Phys. Rev. Lett. **120**, 268001 (2018).